HHS Public Access

Author manuscript

Cell Rep. Author manuscript; available in PMC 2022 February 21.

Published in final edited form as:

Cell Rep. 2022 January 11; 38(2): 110222. doi:10.1016/j.celrep.2021.110222.

Polyamine import and accumulation causes immunomodulation in macrophages engulfing apoptotic cells

Alexandra L. McCubbrey[1,4,7,*], **Shannon A. McManus**[1], **Jazalle D. McClendon**[1], **Stacey M. Thomas**[5], **Hope B. Chatwin**[1], **Julie A. Reisz**[6], **Angelo D'Alessandro**[6], **Kara J. Mould**[1,4], **Donna L. Bratton**[2,3], **Peter M. Henson**[3], **William J. Janssen**[1,4,*]

[1]Division of Pulmonary, Critical Care, and Sleep Medicine, Department of Medicine, Denver, CO 80206, USA

[2]Division of Pediatric Allergy and Clinical Immunology, Department of Pediatrics, Denver, CO 80206, USA

[3]Program in Cell Biology, Department of Pediatrics, National Jewish Health, Denver, CO 80206, USA

[4]Division of Pulmonary Diseases and Critical Care Medicine, Department of Medicine, Aurora, CO 80045, USA

[5]Department of Orthopedics, Aurora, CO 80045, USA

[6]Department of Biochemistry and Molecular Genetics, University of Colorado Denver – Anschutz Medical Campus, Aurora, CO 80045, USA

[7]Lead contact

SUMMARY

Phagocytosis of apoptotic cells, termed efferocytosis, is critical for tissue homeostasis and drives anti-inflammatory programming in engulfing macrophages. Here, we assess metabolites in naive and inflammatory macrophages following engulfment of multiple cellular and non-cellular targets. Efferocytosis leads to increases in the arginine-derived polyamines, spermidine and spermine, *in vitro* and *in vivo*. Surprisingly, polyamine accumulation after efferocytosis does not arise from retention of apoptotic cell metabolites or *de novo* synthesis but from enhanced

*Correspondence: mccubbreya@njhealth.org (A.L.M.), janssenw@njhealth.org (W.J.J.).

AUTHOR CONTRIBUTIONS

A.L.M. designed the study, performed experiments, analyzed data, prepared figures, and wrote the manuscript. S.A.M., J.D.M., S.M.T., and H.B.C. performed experiments. J.A.R. and A.D. analyzed and interpreted metabolomic data and contributed to the manuscript. K.J.M. contributed to the manuscript. D.L.B. and P.M.H. contributed to the manuscript and study design. W.J.J. designed and supervised the study and wrote the manuscript. All authors had access to the study data and approved the final manuscript.

DECLARATION OF INTERESTS

The authors declare no competing interests.

INCLUSION AND DIVERSITY

We worked to ensure sex balance in the selection of non-human subjects. One or more of the authors of this paper self-identifies as a member of the LGBTQ+ community. One or more of the authors of this paper self-identifies as an underrepresented ethnic minority in science.

SUPPLEMENTAL INFORMATION

Supplemental information can be found online at https://doi.org/10.1016/j.celrep.2021.110222.

polyamine import that is dependent on Rac1, actin, and PI3 kinase. Blocking polyamine import prevents efferocytosis from suppressing macrophage interleukin (IL)-1β or IL-6. This identifies efferocytosis as a trigger for polyamine import and accumulation, and imported polyamines as mediators of efferocytosis-induced immune reprogramming.

In brief

McCubbrey et al. show that efferocytosis elicits accumulation of intracellular polyamines, spermidine and spermine, in engulfing macrophages. Efferocytosis does not increase polyamine synthesis but triggers endocytic import of polyamines. Blocking endocytic import prevents polyamine accumulation after efferocytosis and reduces the ability of efferocytosis to suppress IL-1β and IL-6.

Graphical Abstract

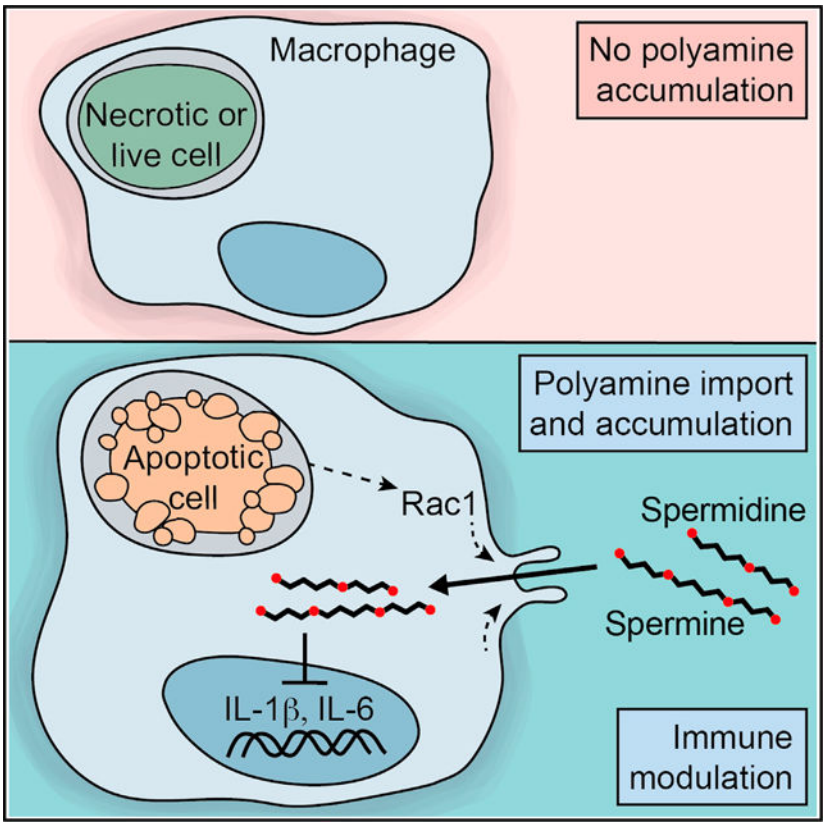

INTRODUCTION

Apoptosis is a constant part of life. In the healthy human body, an estimated 100 billion aged and damaged cells die each day (Nagata, 2018; Arandjelovic and Ravichandran, 2015). These are cleared by phagocytes, primarily macrophages, as part of maintaining homeostasis. Clearance of apoptotic cells, termed efferocytosis, is essential but presents an enormous metabolic burden to the engulfing cell. The uptake of a single apoptotic cell may double the metabolites contained within a macrophage (Han and Ravichandran, 2011).

While these metabolites have been shown to alter macrophage metabolism, their fate has not been completely elucidated.

In the context of inflammation, the scale of apoptosis is dramatically increased. In conjunction, efferocytosis by macrophages also increases. This serves to limit inflammation by removing dying cells before they can release their toxic intracellular contents and also reprograms macrophages for anti-inflammatory roles (Henson, 2017; Boada-Romero et al., 2020). One mechanism by which efferocytosis reprograms macrophages involves lipid metabolites that activate liver X receptor and peroxisome proliferation-activated receptor nuclear receptor transcription factors (Kim et al., 2018; A-Gonzalez et al., 2009; Mukundan et al., 2009). Non-lipid apoptotic-cell-derived metabolites have been shown to regulate macrophage functions such as actin mobilization in the context of interleukin (IL)-4 (Yurdagul et al., 2020), but whether they are a signal for immune reprogramming remains unclear.

In addition to removing apoptotic cells, macrophages ingest cells undergoing other forms of death, including necrosis, and even live cells. Collectively, cells destined for clearance are termed target cells. Multiple types of target cells may be present in a tissue, particularly during inflammation, but anti-inflammatory programming following ingestion is a unique response to apoptotic cells (Cocco and Ucker, 2001; Westman et al., 2019; Henson, 2017). Further, although reprogramming after efferocytosis is connected to phosphatidylserine recognition (Birge et al., 2016), many changes require engulfment (Morioka et al., 2018; Mukundan et al., 2009; Bosurgi et al., 2017) and degradation (Martinez et al., 2011). This suggests apoptotic cell metabolites may be involved.

Changes to macrophage metabolism, particularly increased mitochondrial respiration, have been described following macrophage efferocytosis (Catala et al., 2020; Park et al., 2011; Wang et al., 2017; Zhang et al., 2019). At the same time, efferocytosis upregulates lipid export pathways (Fond et al., 2015) and solute carrier membrane transport proteins (Morioka et al., 2018), suggesting many metabolites may be exported rather than metabolized. Little is known about which metabolites from target cells are retained and how these are repurposed by macrophages for fuel or signaling. Moreover, the degree to which these answers depend on the mode of target-cell death has not been explored.

To address these questions, we performed unbiased metabolomic screens to measure metabolite content in naive and inflammatory macrophages that engulfed apoptotic, necrotic, or live cells. Intriguingly, changes in most classes of metabolites were conserved across target-cell types with the exception of arginine-derived polyamines, spermidine and spermine, which were uniquely increased following efferocytosis. Polyamines are known immunomodulators, able to suppress macrophage production of inflammatory cytokines (Latour et al., 2020; Zhang et al., 1997). Surprisingly, elevated polyamines were not the result of apoptotic cell metabolite retention or *de novo* biosynthesis. Instead, efferocytosing macrophages markedly increased polyamine import through a Rac1 and actin-dependent endocytic process. Blocking polyamine import prevented polyamine accumulation and efferocytosis-driven suppression of IL-1β and IL-6 expression in macrophages following lipopolysaccharide (LPS).

RESULTS

Engulfment of target cells increases macrophage amino acid content

To understand the fate of apoptotic cell metabolites after macrophage engulfment, we first used ultra-high-pressure liquid chromatography-mass spectrometry (UHPLC-MS) to quantify central energy metabolites in inflammatory macrophages that had ingested apoptotic cells. Since macrophages can engulf many types of target cells, particularly in the context of inflammation, we performed identical experiments using two additional target cells: necrotic cells and immunoglobulin (Ig) G antibody-opsonized live cells. All three targets were generated from Jurkat cells (apoptotic Jurkat [ApoJ], necrotic Jurkat [NecJ], IgG-opsonized live Jurkat [IgGJ] cells) (Figure S1A) and were co-cultured with LPS-primed murine peritoneal macrophages for 1 h to allow engulfment (Figure 1A). Macrophages were washed to remove unengulfed targets and incubated for a further 3 or 7 h. Fluorescence-activated cell sorting (FACS) was used to separate macrophages that had or had not taken up target cells, enabling direct comparison of metabolic response to engulfment versus response to exposure (Figures 1A and S1B). Unexposed macrophages (no targets added) were used to provide basal metabolite profiles.

Metabolite profiles showed substantial shifts in engulfing macrophage metabolites following uptake of any of the three targets at 4 and 8 h (Figure 1B). In comparison, profiles from non-engulfing macrophages closely matched unexposed controls, suggesting that exposure without actual uptake has limited impact on macrophage metabolites.

We next explored changes in specific classes of metabolites. Amino acid levels increased in macrophages following target-cell engulfment in a conserved pattern across all three targets. This included large increases in arginine, lysine, and methionine (4- to 10-fold) with no increases in alanine or glycine. Engulfment of non-cell targets did not induce elevated amino acids (Figure S1C). This indicates that amino acid increases following engulfment are a direct consequence of digesting a metabolic load. Increased levels of nucleotide metabolites were also observed in cells in response to all three targets, including cytosine. In comparison, adenosine was decreased. More limited and variable changes were observed in glycolytic and tricarboxylic acid cycle metabolites after target-cell uptake. Subtle increases in itaconate and hexose phosphate were evident, which may relate to previous reports that efferocytosis alters glycolysis and mitochondrial respiration (Zhang et al., 2019; Park et al., 2011; Morioka et al., 2018). The limited amplitude of changes suggests that, in contrast to amino acids, these target-cell-derived metabolites are metabolized or exported from macrophages rapidly after engulfment.

Naive and inflammatory macrophages accumulate intracellular polyamines specifically in response to efferocytosis *in vitro* and *in vivo*

Unlike other metabolites, polyamine metabolites showed patterns that were strikingly target specific. Spermidine and spermine were increased in macrophages that engulfed ApoJ, but not other targets (Figure 1B). Intracellular polyamines can be synthesized *de novo* from arginine (Figure 2A) or obtained via import of extracellular polyamines. Synthesis also requires methionine metabolites (Madeo et al., 2018; Casero et al., 2018). As shown in

Figures 1B, 2B, and 2C, levels of the polyamine precursors arginine, methionine, and ornithine were increased following engulfment of any target cell. However, no changes in the diamine putrescine were observed, and increases in polyamines spermidine and spermine only occurred in response to ApoJ, particularly after engulfment (Figures 2B and 2C).

We confirmed this response persisted with other sources of apoptotic cells and with other macrophages. Spermidine and spermine were increased in LPS-primed murine peritoneal macrophages after engulfment of apoptotic murine thymocytes (Figure S2A), and in LPS-primed human monocyte-derived macrophages and LPS-primed bone marrow-derived macrophages (BMDMs) after engulfment of ApoJ (Figures S2B and S2C). Of note, engulfment of carboxylated latex beads or liposomes, non-cell targets often used to mimic apoptotic cells, did not increase polyamine content (Figure 2D). Taken as a whole, these *in vitro* studies show that polyamines consistently increase in inflammatory macrophages that ingest apoptotic cells.

We next assessed the response of naive macrophages *in vivo*. To mimic homeostatic efferocytosis or phagocytosis, we injected carboxytetramethylrhodamine (TAMRA)-labeled ApoJ or IgGJ into the peritonea of naive mice. Macrophages were recovered 8 h later, and engulfing macrophages selected by FACS. Compared with macrophages from un-injected mice, macrophages that ingested ApoJ had increased intracellular spermidine and spermine (Figure 2E). In contrast, polyamine levels were unchanged in macrophages that ingested IgGJ (Figure 2F). These results show that naive macrophages accumulate polyamines *in vivo* in response to efferocytosis.

To examine the metabolic consequences of efferocytosis by inflammatory macrophages *in vivo*, we designed mixed bone marrow chimera mice to track endogenous apoptotic cell engulfment during acute inflammation. In brief, $CD45.1^+$ wild-type mice were irradiated and reconstituted with a 20:80 mixture of $CD45.1^+$:$CD45.2^+DsRed^+CCR2^{-/-}$ bone marrow. This resulted in mixed chimeras in which macrophages were CD45.2 negative, whereas granulocytes and lymphocytes (i.e., potential apoptotic targets) were $CD45.2^+DsRed^+$ (Figure 2G). Previous work has demonstrated that engulfed DsRed can be detected in the phagosome (A-Gonzalez et al., 2017); accordingly, macrophages that engulfed $DsRed^+$ leukocytes could be identified (Figure 2G). Peritoneal inflammation was initiated with thioglycolate, and 48 h later macrophages were collected and sorted by FACS, as shown in Figure 2G. Engulfing macrophages had higher levels of ornithine, spermidine, and spermine than non-engulfing macrophages (Figure 2H), demonstrating that inflammatory macrophages accumulate polyamines *in vivo* in response to efferocytosis.

Naive and inflammatory macrophages retain amino acids, but not polyamines, from engulfed apoptotic cells

To directly trace the fate of target-cell-derived metabolites in engulfing macrophages, Jurkat cells were cultured in medium containing [^{13}C,^{15}N] amino acids until ^{13}C,^{15}N signal was observed throughout the amino acids and polyamines (Figures S3A–S3B). Isotope-labeled ApoJ were co-cultured with inflammatory macrophages for 1 h (Figure 3A) then washed to remove non-ingested targets. The isotope signal in engulfing versus non-engulfing macrophages was quantified by UHPLC-MS 7 h later. Substantial isotopic

enrichment was detected in amino acids of engulfing macrophages (Figure 3B), while isotope labeling of polyamines was strikingly absent (Figure 3C). This experiment was repeated *in vivo* by injecting isotope-labeled ApoJ into the peritonea of naive mice. Macrophages were recovered 8 h later, and engulfing macrophages were selected by FACS. Engulfing macrophages again showed isotopic enrichment in amino acids but not in polyamines (Figures S3C–S3D). The same pattern was observed in response to injection of isotope-labeled IgGJ (Figures S3C–S3D). These data demonstrate that target-cell-derived amino acids are retained by engulfing macrophages, directly contributing to the overall increase in macrophage amino acid content after target-cell engulfment. However, target-derived polyamines are not retained and do not drive increased spermidine and spermine in macrophages after efferocytosis.

Increased spermidine and spermine do not derive from increased biosynthesis from arginine

Increased arginase expression and activity have been reported in response to efferocytosis (Johann et al., 2007; Bosurgi et al., 2017; Yurdagul et al., 2020). Accordingly, we explored the possibility that efferocytosis enhanced biosynthesis of polyamines from arginine. LPS-primed macrophages were exposed to ApoJ for 1 h, then medium removed and replaced with fresh medium containing [$^{13}C_6$,$^{15}N_4$]arginine (Figure 3D). Engulfing and non-engulfing macrophages were sorted by FACS and ^{13}C,^{15}N labeling in polyamines was assessed. Macrophages cultured in [$^{13}C_6$,$^{15}N_4$]arginine were used as baseline controls. Macrophages constitutively import arginine and [$^{13}C_6$,$^{15}N_4$]arginine was accordingly detected in all groups (Figure S3E). To assess rates of biosynthesis, ratios of ^{13}C,^{15}N labeling between downstream and upstream metabolites were determined (Figures 3E–3G, S3G). Arginase catalysis of arginine yields ornithine, so, to infer flux through arginase, we determined the relative ratio of [$^{13}C_5$,$^{15}N_2$]ornithine within total ornithine to [$^{13}C_6$,$^{15}N_4$]arginine within total arginine. Compared with unexposed control macrophages, the ratio of enriched ornithine:arginine was significantly increased in engulfing macrophages, indicating increased arginase activity (Figure 3E). [$^{13}C_5$,$^{15}N_1$]ornithine was observed but excluded from the numerator as it is not a product of arginase activity, instead forming from other minor pathways of arginine metabolism. Levels of [$^{13}C_5$,$^{15}N_1$]ornithine were very low and unchanged across groups (Figures S3E–S3G).

To infer flux through ornithine decarboxylase (ODC1), we determined the relative ratio of [$^{13}C_4$,$^{15}N_2$]putrescine to [$^{13}C_5$,$^{15}N_2$]ornithine. The ratio of enriched putrescine:ornithine was strongly decreased in engulfing macrophages, implying dampened ODC1 activity following efferocytosis (Figure 3F). No change in the ratio of [$^{13}C_4$,$^{15}N_2$]spermidine to [$^{13}C_4$,$^{15}N_2$]putrescine was observed, suggesting that *de novo* synthesis of spermidine was not increased (Figure 3G). ^{13}C,^{15}N labeling was not detected in spermine, nor citrulline in any group, suggesting minimal spermine synthesis from arginine and minimal arginine metabolism by inducible nitric oxide synthase (iNOS) over the time assessed. Collectively, these data corroborate previous reports that arginine metabolism is changed by efferocytosis, but show that increased spermidine and spermine content in inflammatory macrophages is not the result of biosynthesis from arginine.

Efferocytosis enhances polyamine import from the environment, requiring Rac1 and PI3 kinase

Since intracellular polyamine levels can be regulated by import and export from the environment, we next considered whether efferocytosis increased polyamine import. To test this, we co-cultured LPS-primed peritoneal macrophages with ApoJ for 1 h, removed un-ingested targets, and then added medium containing a fluorescently tagged spermine analog (NBD-spermine) (Guminski et al., 2009) (Figure 4A). NBD-spermine import was significantly increased in macrophages that engulfed ApoJ in contrast to unexposed and non-engulfing macrophages (Figures 4B and 4C). Increased import was also observed in naive BMDMs that engulfed ApoJ (Figure S4A). Importantly, engulfment of IgGJ or carboxylated beads had no impact on macrophage NBD-spermine import (Figures 4B and 4C), congruent with the unique effect of efferocytosis on polyamine accumulation.

Polyamines can be imported into the cell via membrane transport proteins or endocytosis (Madeo et al., 2018; Abdulhussein and Wallace, 2014). To assess the mechanism of import after efferocytosis, targeted inhibitors were added to the media. We first targeted membrane transport proteins using the polyamine transport inhibitor AMXT-1483 ((Burns et al., 2009), compound #10). This partially blocked polyamine import in control macrophages but failed to block the efferocytosis-induced increase in import (Figure 4D). As a next step, different pathways of endocytosis were inhibited. Dynasore, an inhibitor of clathrin-dependent endocytosis (Figure 4H), had no effect on spermine import after efferocytosis. However, import was partially inhibited by cytochalasin D (an inhibitor of actin cytoskeletal reorganization) and strongly inhibited by the Rac1 inhibitor NSC23766, the phosphoinositide 3 (PI3) kinase inhibitor wortmannin, and cold incubation (Figure 4E). NSC23766 also blocked polyamine import by naive BMDMs (Figures S4A–S4B). We next assessed if Rac1-dependent import was activated *in vivo*. We injected naive mice with ApoJ and NBD-spermine with or without NSC23766. Macrophage import of NBD-spermine increased *in vivo* following ApoJ engulfment (Figures 4F and 4G). This increase was inhibited by NSC23766 (Figures 4F and 4G). Taken as a whole, these experiments demonstrate that macrophages import extracellular spermine through Rac1-dependent pinocytosis after efferocytosis *in vitro* and *in vivo*.

To address if this reflected a general increase in fluid-phase endocytosis, we compared import of spermine by naive BMDMs with import of dextran. Spermine and dextran were both imported by macrophages at baseline. However, only import of spermine strongly increased after efferocytosis, which contrasted with limited changes to import of dextran (Figure 4H). These data demonstrate that naive and inflammatory macrophages gain a particular ability to endocytose polyamines after efferocytosis that is dependent on Rac1 but not generalizable to an increase in all fluid-phase endocytosis.

Efferocytosis-enhanced polyamine import drives polyamine accumulation and mediates suppression of IL-1β and IL-6

To confirm that Rac1-mediated import was responsible for polyamine accumulation following efferocytosis, we co-cultured LPS-primed peritoneal macrophages with ApoJ, then treated macrophages with NSC23766 or control media. Macrophage polyamine content

in control, non-engulfing, and engulfing macrophages was measured by UHPLC-MS 7 h later. While macrophages in control medium robustly increased polyamines after efferocytosis, macrophages cultured with NSC23766 showed no increase in spermidine or spermine content (Figure 4I). These data support that Rac1-dependent polyamine import is required for polyamine accumulation after efferocytosis.

Separate studies have connected polyamines and efferocytosis to suppression of pro-inflammatory cytokines (Zhang et al., 1997; Greenlee-Wacker, 2016; Yang et al., 2016; Cocco and Ucker, 2001). Therefore, we asked whether polyamine accumulation was required for efferocytosis-induced suppression of pro-inflammatory cytokine production. Blocking polyamine import in BMDMs with NSC23766 reversed the immunosuppressive effect of efferocytosis on IL-1β and IL-6 transcription in response to LPS (Figures 4J and 4K). Collectively, these data demonstrate that import of environmental polyamines drives polyamine accumulation after efferocytosis and that imported polyamines mediate part of efferocytosis-driven immune reprogramming.

DISCUSSION

Here we assess changes to macrophage intracellular metabolites following engulfment of apoptotic, live, or necrotic cells. Our data show that spermidine and spermine, collectively polyamines, are increased in macrophages *in vitro* and *in vivo* specifically following engulfment of apoptotic cells. Accumulation of intracellular polyamines is driven by increased import of environmental polyamines and mediates the efferocytosis-induced suppression of IL-1β and IL-6.

In these experiments, we describe unique accumulation of polyamines in both naive and inflammatory macrophages after efferocytosis. Polyamines and arginine metabolism have been a focus of macrophage biologists since their association with IL-4 polarized M2 reparative macrophages (Mills et al., 2000; Rath et al., 2014) and continue to be pathways of interest in inflammation and repair (Hardbower et al., 2017; Puleston et al., 2019; Latour et al., 2020; Singh et al., 2018). Although the *in vitro* M1-M2 dichotomy cannot encapsulate the dynamic *in vivo* programming of macrophages (Xue et al., 2014; Martinez and Gordon, 2014), efferocytosis-driven programming is often called M2-like and includes changes to arginine metabolism (Freire-De-Lima et al., 2000; Medina et al., 2020; Yurdagul et al., 2020). To this end, elevated polyamines have been reported in thioglycolate-elicited peritoneal macrophages (Zhang et al., 2019) and IL-4 primed BMDMs (Yurdagul et al., 2020) following efferocytosis *in vitro*. Notably, mechanisms to explain spermidine and spermine increases were not determined in these studies and the response to engulfment of other target cells was not examined. Our study addresses these issues and finds that polyamines increase specifically following engulfment of apoptotic cells through increased polyamine import.

Intracellular polyamine levels reflect a balance of synthesis, catabolism, import, and export (Madeo et al., 2018). Our data support that, at baseline, macrophages both import and synthesize polyamines. Previous work has shown that synthesis is tightly regulated. Antizymes and antizyme inhibitors respond to elevated intracellular polyamines

by suppressing ODC activity (Kahana, 2018). This mechanism may explain the decrease in ODC activity we observed after efferocytosis. Of note, a previous study examined arginine metabolism after efferocytosis in the context of IL-4. IL-4 unlocked the capacity of macrophages to perform repeat engulfments via increasing ODC activity and synthesis of putrescine after efferocytosis (Yurdagul et al., 2020). Our findings are complementary, not inconsistent; differences likely reflect known divergent effects of LPS and IL-4 polarization on arginine metabolism (Rath et al., 2014) and may also relate to differences in the timing when ornithine flux was examined (8 versus 3 h). Importantly, Yurdagul et al. found that loss of ODC blocked the increase in diamine putrescine after efferocytosis but not accumulation of polyamines spermidine and spermine. Thus, *de novo* synthesis explains elevated putrescine but not elevated polyamines in IL-4-polarized BMDMs. Polyamine accumulation in IL-4-polarized macrophages may also involve increased polyamine import.

We show that macrophages increase import of polyamines after efferocytosis *in vitro* and *in vivo*. In the absence of efferocytosis, macrophages rely on membrane transport proteins for a significant portion of import. However, following efferocytosis, endocytic import is upregulated and becomes the dominant mechanism. This does not appear to be due to a general increase in fluid-phase endocytosis, since this increase is not observed for uptake of dextran. However, it is dependent on the actin cytoskeleton, PI3 kinase, and Rac1. Future studies will be critical to determine the mechanisms that regulate efferocytosis-induced polyamine import.

Polyamines and efferocytosis have each been shown to suppress transcription of pro-inflammatory cytokines, including IL-1β, tumor necrosis factor alpha (TNFα), and IL-6 (Zhang et al., 1997; Hardbower et al., 2017; Singh et al., 2018; Erwig and Henson, 2007; Cocco and Ucker, 2001). Our data link these observations by showing that polyamines accumulate after efferocytosis and that blocking accumulation via inhibition of Rac1-dependent import prevents the suppressive effect of efferocytosis on IL-1β and IL-6 expression. This implies that concentrations of polyamines in the local environment may regulate macrophage reprogramming by efferocytosis.

Polyamines are found in the circulation of humans and mice at micromolar concentrations that are influenced by diet and decrease with age (Soda et al., 2009; Madeo et al., 2018). Intriguingly, apoptotic cells themselves release spermidine in a caspase-dependent manner (Medina et al., 2020). We confirmed that conditioned medium from ApoJ contains highly elevated spermidine (Figure S4D). However, this ApoJ-derived environmental contribution was removed in our *in vitro* assays by the wash after co-culture (Figure S4E). We speculate that apoptotic cell release of polyamines could promote import-driven anti-inflammatory reprogramming of macrophages *in vivo*. However, this interaction was not captured in our study design. Further, we predict that, in settings where circulating polyamine levels are low, such as with aging (Madeo et al., 2018), efferocytosis might fail to appropriately suppress inflammatory cytokines. This impairment could contribute to the phenomenon of “inflammaging” (Franceschi et al., 2018).

Polyamines may regulate efferocytosis-driven functional shifts beyond cytokine suppression. Efferocytosis has also been shown to activate pro-repair programming (Henson, 2017;

Bosurgi et al., 2017). This may relate to the requirement of spermidine for synthesis of hypusine (Shin et al., 2017; Madeo et al., 2018), a post-translational modification on the ribosome that increases translation efficiency. Recent work has identified multiple settings where hypusination is critical for macrophage function, including expression of a pro-repair portion of the M2 IL-4 response (Puleston et al., 2019) and control of bacterial infection without exuberant inflammation (Gobert et al., 2020). In this context, we predict that efferocytosis, via triggering accumulation of spermidine, may increase the ability of macrophages to form hypusine.

In summary, spermidine and spermine accumulate in macrophages following efferocytosis of apoptotic cells but not other types of target cells. Accumulation of these two polyamines occurs via Rac1-dependent import from the environment and triggers suppression of pro-inflammatory cytokine production. This identifies a metabolite-driven mechanism for immunosuppression by efferocytosis.

Limitations of the study

Additional experiments are required to understand the significance of polyamine import for macrophage immunomodulation *in vivo*. Inhibition of Rac1, PI3K, or actin movement are blunt tools to disrupt endocytosis and do not identify how efferocytosis causes macrophages to increase import of polyamines with limited effect on dextran. Without clearer mechanism, it remains possible that import of other metabolites or material may occur through this mechanism alongside polyamines, which could affect macrophage function. Further, we have assumed that inhibitors used in this study target the pathways indicated, but off-target effects could be relevant to polyamine import and immune reprogramming. This study was limited to assessing metabolites after engulfment of immune cells by macrophages. We did not test whether engulfment of stromal cells, phagocytosis of bacteria, or enveloped virus entry triggered polyamine import. Key goals for the future include (1) understanding how efferocytosis but not uptake of live or necrotic cells triggers increased polyamine import, (2) clarifying the mechanism of selective polyamine endocytosis, and (3) testing the relevance of increased polyamine import and accumulation for macrophage immune function *in vivo*.

STAR★METHODS

RESOURCE AVAILABILITY

Lead contact—Further information and requests for resources should be directed to and will be fulfilled, when possible, by Lead Contact, Alexandra McCubbrey (mccubbreya@njhealth.org).

Materials availability—This study did not generate new unique reagents.

Data and code availability

- Raw data from UHPLC-MS have been deposited at NMDR Metabolomics Workbench and are publicly available as of the date of publication. Accession numbers are listed in the key resources table.
- No original code was generated during this study.

- Any additional information required to reanalyze the data reported in this paper is available from the lead contact upon request.

EXPERIMENTAL MODEL AND SUBJECT DETAILS

Experimental animals—This study was approved and performed in accordance with the ethical guidelines of the Institutional Animal Care and Use Committee at National Jewish Health. C57BL/6J (000664), B6-CD45.1 (002014) and CCR2KO (004999) mice were obtained from Jackson Laboratories (Bar Harbor, ME, USA). DsRed.T3 mice (available as 006051 at Jackson Labs) were generously shared by the Nagy laboratory (Vintersten et al., 2004). CCR2KO mice were crossed with DsRed mice until double homozygous. Mice used in experiments were between 8–16 weeks of age. Both male and female sex were used in experiments except bone marrow chimera experiments, which used only male mice.

Human tissue—This study used deidentified donor peripheral blood mononuclear cells (PBMC) collected and isolated (Young et al., 2011) by the National Jewish Blood Prep Core (IRB No. HS-1285). Age and sex of deidentified blood donors in this study is not known.

Cell lines—Jurkat (human T lymphocytes, clone E6–1) were obtained from ATCC and cultured in RPMI-1640 (GIBCO) supplemented with 10% heat-inactivated fetal bovine serum (v/v) (GeminiBio), 1X Pen/Strep/Glut, 1mM HEPES, and 100μM Sodium Pyruvate. Cells were cultured in a humidified CO_2 incubator at 37C. The Jurkat cell line was established from peripheral blood of a 14-year-old male diagnosed with T cell leukemia.

Murine primary cell cultures—Peritoneal cells were isolated from naïve mice by lavage with 10mL of PBS containing 0.5mM EDTA. Lavage was estimated to contain 50% macrophages. Peritoneal macrophages were isolated by adhesion purification of lavage cells in RPMI-10 (RPMI-1640 containing 10% heat-inactivated fetal bovine serum (v/v), 1X Pen/Strep/Glut, 1mM HEPES, and 100μM Sodium Pyruvate) plated 1.3×10^6 macrophages/well in 6-well plates for FACS sorting or 4×10^6 macrophage/well in 24-well plates for flow cytometry. Non-adherent cells were removed by washing after 3–5 hours, and macrophages were cultured in fresh RPMI-10 overnight. 400ng/mL purified *E. coli* O111:B4 LPS (List Biological Laboratories Inc.) was added to generate inflammatory macrophages 12h before the addition of target cells. Bone marrow-derived macrophages were generated by 8-day culture of murine bone marrow cells grown in media containing M-CSF (High glucose DMEM containing 10% v/v FBS, 20% v/v L929-conditioned media, 1X Pen/Strep/Glut, 100μM Sodium Pyruvate, 55μM beta-Mercaptoethanol). All macrophages were removed from culture dishes by 3-minute incubation with 1X Trypsin-EDTA (Sigma) plus gentle scraping.

Human primary cell culture—Human monocyte-derived macrophages (HMDM) were generated from donor peripheral blood mononuclear cells (PBMC). PBMC were differentiated into HMDM by culture in X-Vivo10 (Lonza) containing 10% human serum (pooled from deidentified donors and heat inactivated, National Jewish Health Blood Prep Core) for 7 days. HMDM were plated at 1.3×10^6 macrophages/well in 6-well plates for FACS sorting. 400ng/mL purified *E. coli* O111:B4 LPS (List Biological Laboratories Inc.)

was added to generate inflammatory macrophages 12h before the addition of target cells. HMDM were removed from culture dishes by 3-minute incubation with 1X Trypsin-EDTA (Sigma) plus gentle scraping.

METHOD DETAILS

Apoptotic target cells—Live Jurkat cells in RPMI-10 were exposed to 60,000 μJ of UV energy on a UV Stratalinker 2400 (Stratagene), then incubated at 37C for 4h to generate apoptotic Jurkat cells (ApoJ). Thymocytes, obtained by crushing WT murine thymi and filtering for a single cell suspension, were converted to apoptotic thymocytes in the same manner. For TAMRA-labeling, apoptotic targets were stained during the final hour by 15 minute incubation at 37C with 10μM 5(6)-TAMRA,SE (Invitrogen) in PBS followed by two washes with RPMI-10 to remove excess TAMRA. Apoptotic targets were resuspended in fresh RPMI-10 and added to macrophages in culture at a ratio of 5:1 and co-cultured for 1h. Unengulfed targets were removed by washing macrophages three times with cold 1X PBS. To assess *in vivo* uptake of exogenous targets, 2×10^6 ApoJ were injected IP.

Other cell targets—Jurkat cells destined to be IgGJ and NecJ were TAMRA-labeled prior to opsonization or killing using the procedure described above. Labeled cells were incubated for 30 minutes on ice with 25μg/mL purified anti-human CD3 (Biolegend, Clone UCHT1) to generate IgGJ or incubated for 25 minutes at 55C to generate NecJ. All targets were resuspended in RPMI-10. IgG targets were added to macrophages at a ratio of 4:1 and co-cultured for 1h, NecJ targets were added to macrophages at a ratio of 5:1 and co-cultured for 1h. Unengulfed targets were removed by washing macrophages three times with cold 1X PBS. To assess *in vivo* uptake of exogenous targets, 2×10^6 IgGJ were injected IP.

Non-cell targets—1-Palmitoyl-2-oleoyl-sn-glycero-3-phospho-L-serine (POPS) and 1-palmitoyl-2-oleoyl-glycero-3-phosphocholine (POPC) (Avanti Polar Lipids Inc.) were used to generate PS-containing liposomes. Lipids suspended in chloroform were mixed at 70:30 POPC:POPS, then chloroform was evaporated under nitrogen. Dry lipids were resuspended in RPMI for a final concentration of 500μM lipid and sonicated for 15 minutes until liposomes were formed and solution transitioned from opaque to clear. Liposomes were added to macrophages at a final concentration of 50μM in RPMI-10. For other experiments, Flash Red 5μm carboxylated polystyrene beads (PS/DVB-COOH·(660,690) carboxyl polystyrene beads, Bangs Laboratories Inc.) were added to macrophages at a final ratio of 1:2. Macrophages were co-cultured with non-cell targets for 1h and unengulfed targets were removed by washing macrophages three times with cold 1X PBS.

Isotope-labeled metabolite use—For some experiments, Jurkat T cells were cultured for 4 days in media containing [^{13}C,^{15}N]cell-free amino acid mixture (Sigma-Aldrich) (RPMI-1640 medium for SILAC, 10% v/v dyalized FBS, 1X Pen/Strep, 1mM HEPES, 4% v/v amino acid mixture). For some experiments, macrophages were cultured for 7 hours in media containing [^{13}C,^{15}N]Arginine (Cambridge Isotope Laboratories): RPMI-1640 medium for SILAC, 10% dyalized FBS v/v, 1X Pen/Strep, 1mM HEPES, 100μM Sodium Pyruvate, 0.2 g/L [^{13}C,^{15}N] Arginine.

FACS sorting engulfing and non-engulfing cells—Single cell suspensions were incubated with unlabeled CD16/CD32 for 5 min to block non-specific Fcγ R-mediated binding. Cells were stained with surface antibody panels for 20 min, and then washed. Cells were protected from light and incubations were performed on ice. HBSS containing 0.3% BSA and 0.3 mM EDTA was used as a buffer for all incubations. DAPI was added to cells immediately prior to sort to distinguish live and dead cells. For all *in vitro* target cell engulfment assays, live macrophages (murine peritoneal macrophages: $CD45^+F4/80^+DAPI^-$; murine BMDM: $CD45^+CD88^+DAPI^-$; HMDM: $CD45^+HLA\text{-}DR^+DAPI^-$) were separated into engulfing ($TAMRA^+$) and non-engulfing ($TAMRA^-$) populations. For *in vivo* IP ApoJ or IgGJ engulfment assays, live macrophages were identified as $CD45^+Ly6G^-CD88^+CD11b^+F4/80^{hi}DAPI^-$ and $TAMRA^+$ or $TAMRA^-$. For bead engulfment assays, live macrophages ($CD45^+F4/80^+DAPI^-$) were sorted into engulfing ($Flash\ Red^+$) and non-engulfing ($Flash\ Red^-$) populations. Liposomes had no label; liposome-fed macrophages were only sorted for viability. Primary antibodies used (source/clone): unlabeled CD16/32 (eBioscience/93), Ly6G (BD/IA8), F4/80 (ebioscience/BM8), CD45 (BD/30-F11), CD11b (eBioscience/M1/70), CD88 (BioLegend/20/70), CD64 (Biolegend/X54–5/7.1). All primary antibodies were used at a 1:400 dilution. All macrophages were sorted into 0.06% BSA-coated tubes on a Synergy cell sorter (Sony Biotech).

Generating and FACS sorting bone marrow chimeras—Recipient CD45.1+ mice were lethally irradiated with 900rad using a Cesium-source irradiator. 6h later, recipient mice were given 10×10^6 mixed bone marrow cells by tail vein injection: 80% $CCR2^{-/-}DsRed^+CD45.2^+$ marrow and 20% $CD45.1^+$ marrow. New marrow was allowed to engraft for 6 weeks, then mice were challenged with 1mL of 4% thioglycolate given IP. Peritoneal lavage was collected 48h after thioglycolate; live macrophages were identified ($CD45.1^+CD45.2^-Ly6G^-CD11b^+CD64^+F4/80^{hi}DAPI^-$), then separated into engulfing ($DsRed^+$) and non-engulfing ($DsRed^-$) populations using the FACS sorting process described above. Blood neutrophils and lymphocytes were verified by flow cytometry as 80% $DsRed^+$.

Metabolomics—To process cells for assessment of intracellular metabolites, cells were pelleted at 400×g in tubes coated with 0.06% BSA. Supernatant was aspirated and discarded; residual liquid was carefully wicked away from the pellet with a kimwipe. Dry pellets were immediately snap frozen and stored at −80C until processing. To process culture supernatants for assessment of metabolites, supernatant was centrifuged at 400×g to pellet any cells. Cell-free supernatant was then transferred to a fresh tube, snap frozen, and stored at −80C until processing. Ultra-high pressure liquid chromatography-mass spectrometry (UHPLC-MS) was performed by the University of Colorado School of Medicine Metabolomics Core. Metabolites from frozen cell pellets were extracted at 2e6 cells/mL in ice cold 5:3:2 MeOH:acetonitrile:water (v/v/v). Media was thawed on ice and a 10 μL aliquot treated with 240 μL of the same extraction solution. Extractions were carried out using vigorous vortexing for 30 min at 4C. Supernatants were clarified by centrifugation (10 min, 18,000 g, 4C) and analyzed using a Thermo Vanquish UHPLC coupled to a Thermo Q Exactive mass spectrometer. Global metabolomics analyses were

performed using a 3 min isocratic run in positive and negative ion modes (separate runs) as described previously (Nemkov et al., 2015, 2017); stable isotope tracing samples were analyzed using a 5 min C18 gradient in positive and negative ion modes (separate runs) as described (Nemkov et al., 2019; Gehrke et al., 2019). For all analyses, the MS scanned in MS^1 mode across the m/z range of 65 to 950. Peaks were annotated (in conjunction with the KEGG database), integrated, and quality control performed using Maven (Princeton University) as described. Stable isotope tracing results were isotopically corrected for the natural abundance of $^{13}C_1$, $^{13}C_2$, $^{15}N_1$, and $^{15}N_2$ (Nemkov et al., 2017).

Polyamine or dextran import flow cytometry assay—Murine peritoneal macrophages were plated, primed with LPS, and co-cultured with ApoJ, IgGJ, or carboxylated beads as described above. For same experiments naïve BMDM were co-cultured with ApoJ. Following removal of unengulfed ApoJ by repeated washing with PBS, 1.5μM *N*(1)-Methylspermine NBD conjugate 5 (Guminski et al., 2009) (NBD-spermine) or 2μg/mL 10,000 MW AF647-Dextran (Invitrogen) was added to macrophages in RPMI-10 and incubated for 7h. NBD-spermine was generously provided by Mark Burns (Aminex Therapeutics, Newcastle, WA). For some experiments, macrophages were treated with inhibitors. 1μM AMXT-1483 ((Burns et al., 2009), Compound #10) (Aminex Therapeutics, Newcastle, WA) was used starting 4h before the addition of ApoJ. All other inhibitors were used starting immediately after removal of ApoJ and 30 minutes prior to adding NBD-Spermine or Dextran: 10μM cytochalasin D (Invitrogen), 100μM NSC23766 (Sigma-Aldrich), 80μM Dynasore (Sigma-Aldrich), or 100nM Wortmannin (Sigma-Aldrich). Inhibitors remained in culture continually once added. For some experiments, macrophages were immediately moved to 4C upon addition of NBD-spermine or Dextran. After 7h of incubation with NBD-spermine or Dextran, extracellular tracer was removed by washing wells 5 times with cold PBS. Then macrophages were harvested, stained with CD88 surface antibody, and DAPI was added to distinguish live and dead cells as described above. To assess *in vivo* polyamine import mice were injected IP with 2×10^6 ApoJ. 1h later, some mice were injected IP with 5mg/kg NSC23766. 30 minutes later, mice were injected IP with 45 nmol of NBD-spermine. Peritoneal lavage was harvested 5h later and cells stained as described above. Stained cells were analyzed using an LSRII flow cytometer (BD) and FlowJo software (Tree Star, Ashland, OR, USA) to separate engulfing from non-engulfing macrophages and assess the median fluorescence index of NBD-spermine or Dextran in each population.

Gene expression—Murine bone marrow-derived macrophages were plated and co-cultured with ApoJ for 1h. Following removal of unengulfed ApoJ by repeated washing with PBS, macrophages were treated with 400ng/mL purified *E. coli* O111:B4 LPS (List Biological Laboratories Inc.) ± 100μM NSC23766 for 6h, then RNA was collected and isolated using the RNeasy micro isolation kit (QIAGEN) per the manufacturer's instructions. RT-PCR was performed using the SensiFAST Probe Hi-ROX One-Step Kit (Meridian Life Science Inc.) per manufacturer's instructions with Taqman gene expression assay primers (Invitrogen). Expression of *il-1b* (Assay ID: Mm99999061_mH) *and il-6* (Assay ID: Mm00446190_m1) was normalized to *b2m* (Assay ID: Mm00437762_m1).

QUANTIFICATION AND STATISTICAL ANALYSIS

One-way ANOVA with Dunnett's multiple comparison test or unpaired t test was used to analyze differences between data groups. The data are presented as mean ± standard error of the mean (SEM) and were considered statistically significant when $p < 0.05$. In figure legends, n represents number of individual samples. Study design involved at least two independent experiments. Exclusion criteria prior to the start of any exogenous or endogenous *in vivo* engulfment studies were death, injury requiring euthanasia, or weight loss > 20%. All statistical analyses were conducted using GraphPad Prism, Version 7.0d (GraphPad Inc., CA, USA).

Supplementary Material

Refer to Web version on PubMed Central for supplementary material.

ACKNOWLEDGMENTS

Thanks to Josh Loomis at the National Jewish Flow Cytometry Core for assistance with FACS; thanks to Benjamin C. Brown, Rachel Culp-Hill, and Eric Bohrnsen at the University of Colorado School of Medicine Metabolomics Core for assistance with metabolomics experiments; and thanks to Dr. Mark Burns and Aminex Therapeutics Incorporated for sharing reagents. Grant support: NIH K99HL141658 (A.L.M.), NIH R00HL141658 (A.L.M.), NIH K08 20115802 (K.J.M.), NIH R01AI141389 (D.L.B.), NIH R01HL149741 (P.M.H.), NIH R35HL140039 (W.J.J.), and NIH R01HL130938 (W.J.J.).

REFERENCES

A-Gonzalez N, Bensinger SJ, Hong C, Beceiro S, Bradley MN, Zelcer N, Deniz J, Ramirez C, Díaz M, Gallardo G, et al. (2009). Apoptotic cells promote their own clearance and immune tolerance through activation of the nuclear receptor LXR. Immunity 31, 245–258. [PubMed: 19646905]

A-Gonzalez N, Quintana JA, García-Silva S, Mazariegos M, González De La Aleja A, Nicolás-Ávila JA, Walter W, Adrover JM, Crainiciuc G, Kuchroo VK, et al. (2017). Phagocytosis imprints heterogeneity in tissue-resident macrophages. J. Exp. Med. 214, 1281–1296. [PubMed: 28432199]

Abdulhussein AA, and Wallace HM (2014). Polyamines and membrane transporters. Amino Acids 46, 655–660. [PubMed: 23851697]

Arandjelovic S, and Ravichandran KS (2015). Phagocytosis of apoptotic cells in homeostasis. Nat. Immunol. 16, 907–917. [PubMed: 26287597]

Birge RB, Boeltz S, Kumar S, Carlson J, Wanderley J, Calianese D, Barcinski M, Brekken RA, Huang X, Hutchins JT, et al. (2016). Phosphatidylserine is a global immunosuppressive signal in efferocytosis, infectious disease, and cancer. Cell Death Differ. 23, 962–978. [PubMed: 26915293]

Boada-Romero E, Martinez J, Heckmann BL, and Green DR (2020). The clearance of dead cells by efferocytosis. Nat. Rev. Mol. Cell Biol. 21, 398–414. [PubMed: 32251387]

Bosurgi L, Cao YG, Cabeza-Cabrerizo M, Tucci A, Hughes LD, Kong Y, Weinstein JS, Licona-Limon P, Schmid ET, Pelorosso F, et al. (2017). Macrophage function in tissue repair and remodeling requires IL-4 or IL-13 with apoptotic cells. Science 356, 1072–1076. [PubMed: 28495875]

Burns MR, Graminski GF, Weeks RS, Chen Y, and O'Brien TG (2009). Lipophilic lysine-spermine conjugates are potent polyamine transport inhibitors for use in combination with a polyamine biosynthesis inhibitor. J. Med. Chem. 52, 1983–1993. [PubMed: 19281226]

Casero RA JR., Murray Stewart T, and Pegg AE (2018). Polyamine metabolism and cancer: treatments, challenges and opportunities. Nat. Rev. Cancer 18, 681–695. [PubMed: 30181570]

Catala A, Youssef LA, Reisz JA, Dzieciatkowska M, Powers NE, Marchetti C, Karafin M, Zimring JC, Hudson KE, Hansen KC, et al. (2020). Metabolic reprogramming of mouse bone marrow derived macrophages following erythrophagocytosis. Front Physiol. 11, 396. [PubMed: 32425810]

Cocco RE, and Ucker DS (2001). Distinct modes of macrophage recognition for apoptotic and necrotic cells are not specified exclusively by phosphatidylserine exposure. Mol. Biol. Cell 12, 919–930. [PubMed: 11294896]

Erwig LP, and Henson PM (2007). Immunological consequences of apoptotic cell phagocytosis. Am. J. Pathol. 171, 2–8. [PubMed: 17591947]

Fond AM, Lee CS, Schulman IG, Kiss RS, and Ravichandran KS (2015). Apoptotic cells trigger a membrane-initiated pathway to increase ABCA1. J. Clin. Invest. 125, 2748–2758. [PubMed: 26075824]

Franceschi C, Garagnani P, Parini P, Giuliani C, and Santoro A (2018). Inflammaging: a new immune-metabolic viewpoint for age-related diseases. Nat. Rev. Endocrinol. 14, 576–590. [PubMed: 30046148]

Freire-De-Lima CG, Nascimento DO, Soares MB, Bozza PT, Castro-Faria-Neto HC, De Mello FG, Dosreis GA, and Lopes MF (2000). Uptake of apoptotic cells drives the growth of a pathogenic trypanosome in macrophages. Nature 403, 199–203. [PubMed: 10646605]

Gehrke S, Rice S, Stefanoni D, Wilkerson RB, Nemkov T, Reisz JA, Hansen KC, Lucas A, Cabrales P, Drew K, and D'Alessandro A (2019). Red blood cell metabolic responses to torpor and arousal in the hibernator arctic ground squirrel. J. Proteome Res. 18, 1827–1841. [PubMed: 30793910]

Gobert AP, Finley JL, Latour YL, Asim M, Smith TM, Verriere TG, Barry DP, Allaman MM, Delagado AG, Rose KL, et al. (2020). Hypusination orchestrates the antimicrobial response of macrophages. Cell Rep 33, 108510. [PubMed: 33326776]

Greenlee-Wacker MC (2016). Clearance of apoptotic neutrophils and resolution of inflammation. Immunol. Rev. 273, 357–370. [PubMed: 27558346]

Guminski Y, Grousseaud M, Cugnasse S, Brel V, Annereau JP, Vispé S, Guilbaud N, Barret JM, Bailly C, and Imbert T (2009). Synthesis of conjugated spermine derivatives with 7-nitrobenzoxadiazole (NBD), rhodamine and bodipy as new fluorescent probes for the polyamine transport system. Bioorg. Med. Chem. Lett. 19, 2474–2477. [PubMed: 19332372]

Han CZ, and Ravichandran KS (2011). Metabolic connections during apoptotic cell engulfment. Cell 147, 1442–1445. [PubMed: 22196723]

Hardbower DM, Asim M, Luis PB, Singh K, Barry DP, Yang C, Steeves MA, Cleveland JL, Schneider C, Piazuelo MB, et al. (2017). Ornithine decarboxylase regulates M1 macrophage activation and mucosal inflammation via histone modifications. Proc. Natl. Acad. Sci. U S A. 114, E751–E760. [PubMed: 28096401]

Henson PM (2017). Cell removal: efferocytosis. Annu. Rev. Cell Dev Biol. 33, 127–144. [PubMed: 28613937]

Johann AM, Barra V, Kuhn AM, Weigert A, Von Knethen A, and Brüne B (2007). Apoptotic cells induce arginase II in macrophages, thereby attenuating NO production. FASEB J 21, 2704–2712. [PubMed: 17456784]

Kahana C (2018). The antizyme family for regulating polyamines. J. Biol. Chem. 293, 18730–18735. [PubMed: 30355739]

Kim MJ, Lee YJ, Yoon YS, Kim M, Choi JH, Kim HS, and Kang JL (2018). Apoptotic cells trigger the ABCA1/STAT6 pathway leading to PPAR-g expression and activation in macrophages. J. Leukoc. Biol. 103, 885–895. [PubMed: 29603355]

Latour YL, Gobert AP, and Wilson KT (2020). The role of polyamines in the regulation of macrophage polarization and function. Amino Acids 52, 151–160. [PubMed: 31016375]

Madeo F, Eisenberg T, Pietrocola F, and Kroemer G (2018). Spermidine in health and disease. Science 359, eaan2788. [PubMed: 29371440]

Martinez FO, and Gordon S (2014). The M1 and M2 paradigm of macrophage activation: time for reassessment. F1000Prime Rep. 6, 13. [PubMed: 24669294]

Martinez J, Almendinger J, Oberst A, Ness R, Dillon CP, Fitzgerald P, Hengartner MO, and Green DR (2011). Microtubule-associated protein 1 light chain 3 alpha (LC3)-associated phagocytosis is required for the efficient clearance of dead cells. Proc. Natl. Acad. Sci. U S A. 108, 17396–17401. [PubMed: 21969579]

Medina CB, Mehrotra P, Arandjelovic S, Perry JSA, Guo Y, Morioka S, Barron B, Walk SF, Ghesquière B, Krupnick AS, et al. (2020). Metabolites released from apoptotic cells act as tissue messengers. Nature 580, 130–135. [PubMed: 32238926]

Mills CD, Kincaid K, Alt JM, Heilman MJ, and Hill AM (2000). M-1/M-2 macrophages and the Th1/Th2 paradigm. J. Immunol. 164, 6166–6173. [PubMed: 10843666]

Morioka S, Perry JSA, Raymond MH, Medina CB, Zhu Y, Zhao L, Serbulea V, Onengut-Gumuscu S, Leitinger N, Kucenas S, et al. (2018). Efferocytosis induces a novel SLC program to promote glucose uptake and lactate release. Nature 563, 714–718. [PubMed: 30464343]

Mukundan L, Odegaard JI, Morel CR, Heredia JE, Mwangi JW, Ricardo-Gonzalez RR, Goh YP, Eagle AR, Dunn SE, Awakuni JU, et al. (2009). PPAR-delta senses and orchestrates clearance of apoptotic cells to promote tolerance. Nat. Med. 15, 1266–1272. [PubMed: 19838202]

Nagata S (2018). Apoptosis and clearance of apoptotic cells. Annu. Rev. Immunol. 36, 489–517. [PubMed: 29400998]

Nemkov T, D'Alessandro A, and Hansen KC (2015). Three-minute method for amino acid analysis by UHPLC and high-resolution quadrupole orbitrap mass spectrometry. Amino Acids 47, 2345–2357. [PubMed: 26058356]

Nemkov T, Hansen KC, and D'Alessandro A (2017). A three-minute method for high-throughput quantitative metabolomics and quantitative tracing experiments of central carbon and nitrogen pathways. Rapid Commun. Mass Spectrom. 31, 663–673. [PubMed: 28195377]

Nemkov T, Reisz JA, Gehrke S, Hansen KC, and D'Alessandro A (2019). High-throughput metabolomics: isocratic and gradient mass spectrometry-based methods. Methods Mol. Biol. 1978, 13–26. [PubMed: 31119654]

Park D, Han CZ, Elliott MR, Kinchen JM, Trampont PC, Das S, Collins S, Lysiak JJ, Hoehn KL, and Ravichandran KS (2011). Continued clearance of apoptotic cells critically depends on the phagocyte Ucp2 protein. Nature 477, 220–224. [PubMed: 21857682]

Puleston DJ, Buck MD, Klein Geltink RI, Kyle RL, Caputa G, O'Sullivan D, Cameron AM, Castoldi A, Musa Y, Kabat AM, et al. (2019). Polyamines and eIF5A hypusination modulate mitochondrial respiration and macrophage activation. Cell Metab. 30, 352–363.e8. [PubMed: 31130465]

Rath M, Muller I, Kropf P, Closs EI, and Munder M (2014). Metabolism via arginase or nitric oxide synthase: two competing arginine pathways in macrophages. Front Immunol. 5, 532. [PubMed: 25386178]

Shin BS, Katoh T, Gutierrez E, Kim JR, Suga H, and Dever TE (2017). Amino acid substrates impose polyamine, eIF5A, or hypusine requirement for peptide synthesis. Nucleic Acids Res. 45, 8392–8402. [PubMed: 28637321]

Singh K, Coburn LA, Asim M, Barry DP, Allaman MM, Shi C, Washington MK, Luis PB, Schneider C, Delgado AG, et al. (2018). Ornithine decarboxylase in macrophages exacerbates colitis and promotes colitis-associated colon carcinogenesis by impairing M1 immune responses. Cancer Res. 78, 4303–4315. [PubMed: 29853605]

Soda K, Kano Y, Sakuragi M, Takao K, Lefor A, and Konishi F (2009). Long-term oral polyamine intake increases blood polyamine concentrations. J. Nutr. Sci. Vitaminol. (Tokyo) 55, 361–366. [PubMed: 19763038]

Vintersten K, Monetti C, Gertsenstein M, Zhang P, Laszlo L, Biechele S, and Nagy A (2004). Mouse in red: red fluorescent protein expression in mouse ES cells, embryos, and adult animals. Genesis 40, 241–246. [PubMed: 15593332]

Wang Y, Subramanian M, Yurdagul A JR., Barbosa-Lorenzi VC, Cai B, De Juan-Sanz J, Ryan TA, Nomura M, Maxfield FR, and Tabas I (2017). Mitochondrial fission promotes the continued clearance of apoptotic cells by macrophages. Cell 171, 331–345.e22. [PubMed: 28942921]

Westman J, Grinstein S, and Marques PE (2019). Phagocytosis of necrotic debris at sites of injury and inflammation. Front Immunol. 10, 3030. [PubMed: 31998312]

Xue J, Schmidt SV, Sander J, Draffehn A, Krebs W, Quester I, De Nardo D, Gohel TD, Emde M, Schmidleithner L, et al. (2014). Transcriptome-based network analysis reveals a spectrum model of human macrophage activation. Immunity 40, 274–288. [PubMed: 24530056]

Yang Q, Zheng C, Cao J, Cao G, Shou P, Lin L, Velletri T, Jiang M, Chen Q, Han Y, et al. (2016). Spermidine alleviates experimental autoimmune encephalomyelitis through inducing inhibitory macrophages. Cell Death Differ. 23, 1850–1861. [PubMed: 27447115]

Young RL, Malcolm KC, Kret JE, Caceres SM, Poch KR, Nichols DP, Taylor-Cousar JL, Saavedra MT, Randell SH, Vasil ML, et al. (2011). Neutrophil extracellular trap (NET)-mediated killing of Pseudomonas aeruginosa: evidence of acquired resistance within the CF airway, independent of CFTR. PLoS One 6, e23637. [PubMed: 21909403]

Yurdagul A Jr., Subramanian M, Wang X, Crown SB, Ilkayeva OR, Darville L, Kolluru GK, Rymond CC, Gerlach BD, Zheng Z, et al. (2020). Macrophage metabolism of apoptotic cell-derived arginine promotes continual efferocytosis and resolution of injury. Cell Metab. 31, 518–533.e10. [PubMed: 32004476]

Zhang M, Caragine T, Wang H, Cohen PS, Botchkina G, Soda K, Bianchi M, Ulrich P, Cerami A, Sherry B, and Tracey KJ (1997). Spermine inhibits proinflammatory cytokine synthesis in human mononuclear cells: a counterregulatory mechanism that restrains the immune response. J. Exp. Med. 185, 1759–1768. [PubMed: 9151701]

Zhang S, Weinberg S, Deberge M, Gainullina A, Schipma M, Kinchen JM, Ben-Sahra I, Gius DR, Yvan-Charvet L, Chandel NS, et al. (2019). Efferocytosis fuels requirements of fatty acid oxidation and the electron transport chain to polarize macrophages for tissue repair. Cell Metab. 29, 443–456.e5. [PubMed: 30595481]

Highlights

- Efferocytosis triggers macrophages to accumulate polyamines spermidine and spermine
- Polyamine accumulation is mediated by Rac1-dependent endocytic import
- Inhibition of polyamine import blunts immunomodulation in response to efferocytosis

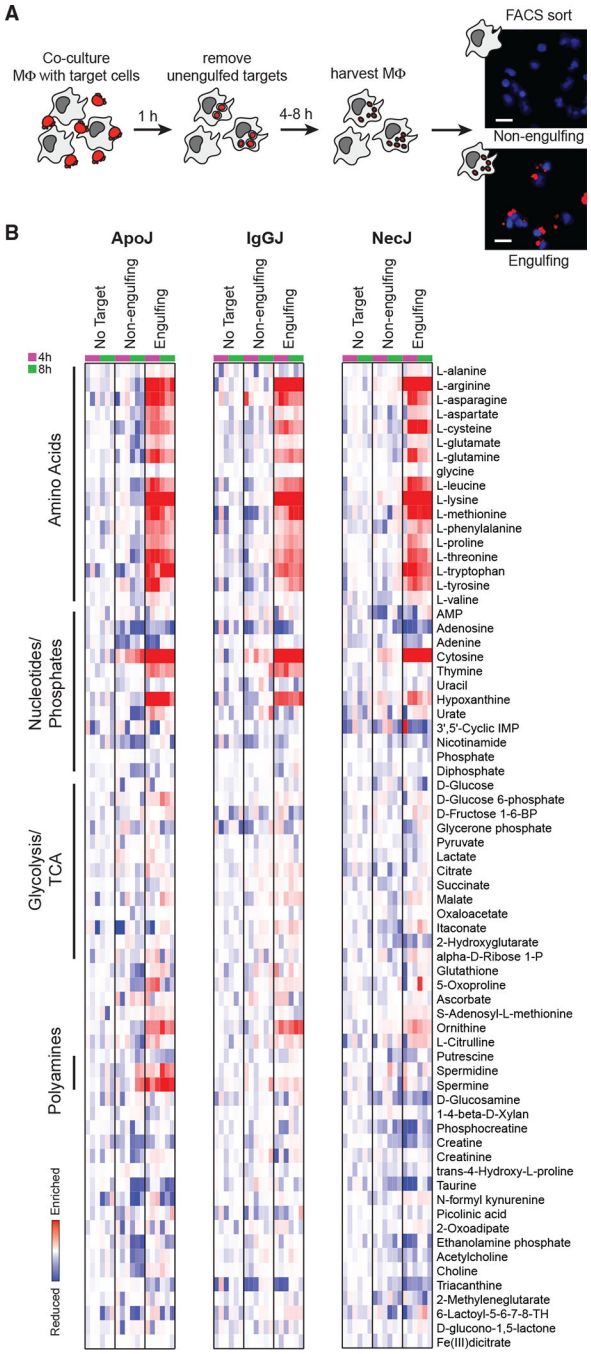

Figure 1. UHPLC-MS identifies intracellular metabolites in macrophages after engulfment of apoptotic, live, or necrotic target cells

(A) Timeline for co-culture and sorting.

(B) LPS-primed murine peritoneal macrophages were cultured alone (no target) or co-cultured with ApoJ, (IgGJ), or NecJ Jurkat cells, then FACS sorted into non-engulfing and engulfing populations. Macrophage metabolites were assessed using UHPLC-MS. Heatmaps show intracellular metabolite levels after target-cell engulfment relative to the no-target group (red, enriched; blue, reduced). Two time points were assessed (4 h, pink; 8 h, green) with n = 3 replicates at each time point. Scale bars in microscopy images represent 25 μm.

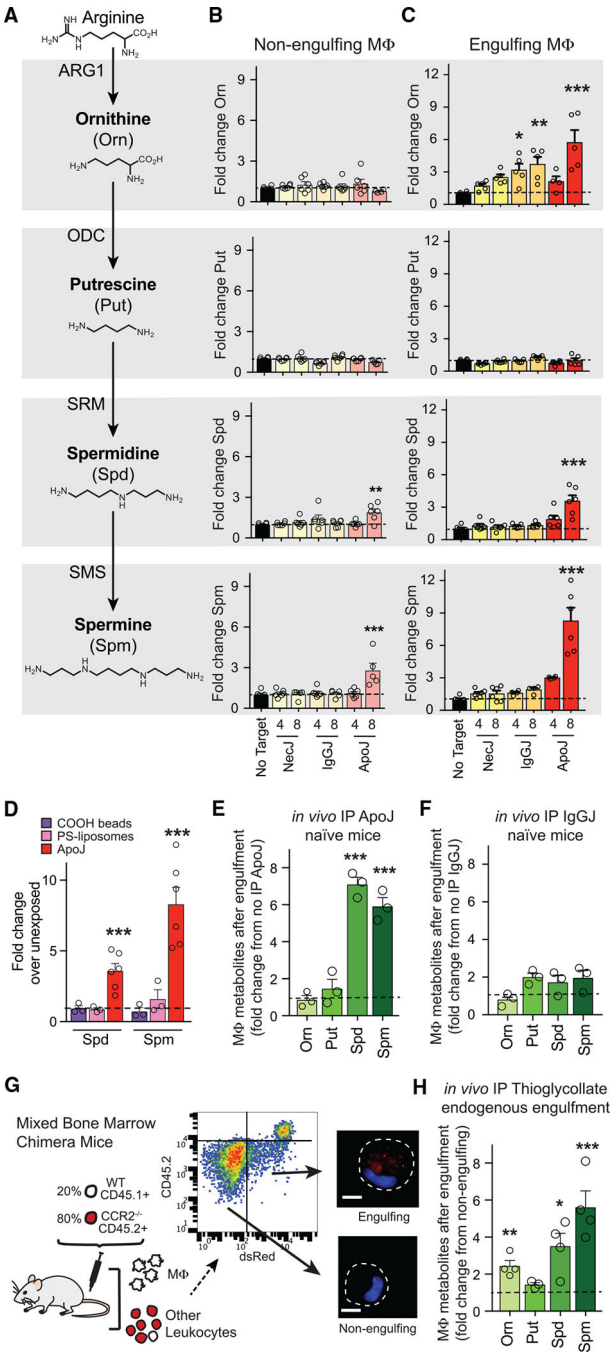

Figure 2. Polyamines accumulate in macrophages after efferocytosis but not in response to engulfment of other target cells *in vitro* and *in vivo*

(A) Polyamine synthesis pathway from arginine.

(B and C) Metabolites in (B) non-engulfing and (C) engulfing LPS-primed murine peritoneal macrophages after co-culture with target cells. n = 5.

(D) Metabolites in LPS-primed peritoneal macrophages co-cultured with PS-containing liposomes or carboxylated latex beads. Data show fold change of PS-liposome exposed macrophages or carboxylated bead engulfing unexposed macrophages (ApoJ target response included for comparison). n = 3–6.

(E) ApoJ were injected intraperitoneally (IP) into naive mice. Engulfing peritoneal macrophages were collected 8 h later; metabolites were compared with control macrophages from un-injected mice. n = 3.

(F) IgGJ were injected IP into naive mice. Engulfing peritoneal macrophages were collected 8 h later; metabolites were compared with control macrophages from un-injected mice. n = 3.

(G and H) Bone marrow chimeras were generated to track endogenous apoptotic cell engulfment.

(G) Mixed bone marrow chimera scheme to generate mice with representative FACS showing cytospin images of sorted non-engulfing and engulfing peritoneal macrophages. Scale bars in microscopy images represent 10 μm.

(H) Mixed bone marrow chimeras were treated with IP thioglycolate and lavage harvested after 48 h. Metabolites from $CD45.1^{+}$ $CD45.2^{-}DsRed^{+}$ engulfing macrophages were compared with metabolites from $CD45.1^{+}CD45.2^{-}DsRed^{-}$ non-engulfing macrophages. n = 4. Data are shown as mean ± standard error of the mean (SEM); *p < 0.05, **p < 0.01, ***p < 0.001.

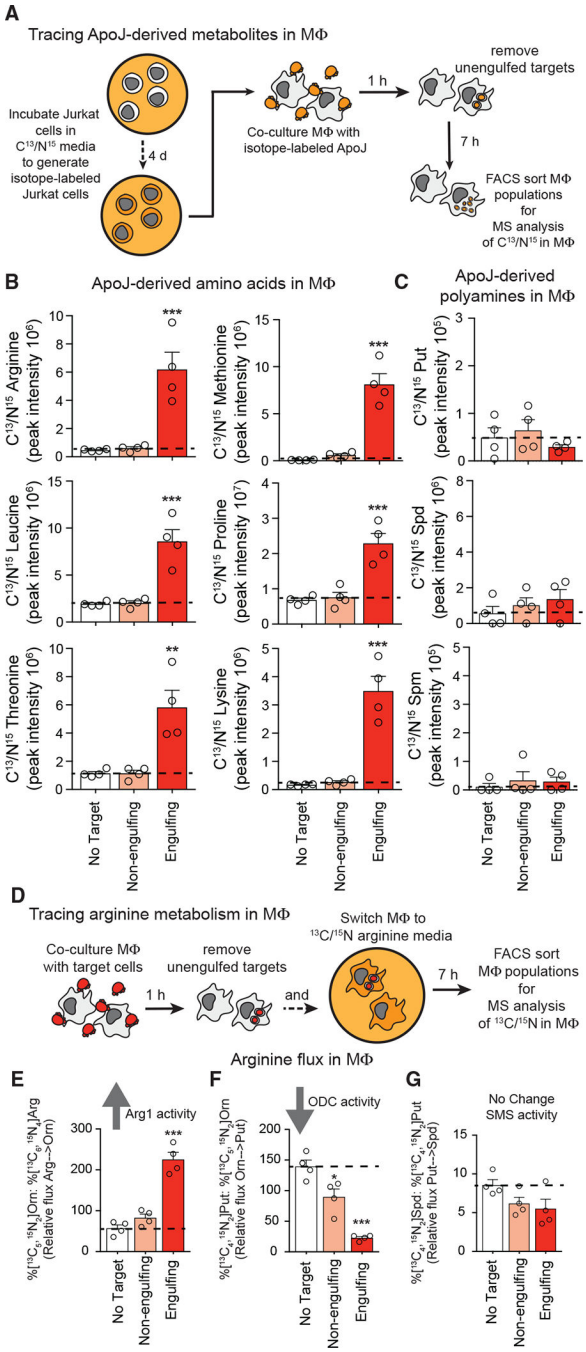

Figure 3. Target-cell-derived amino acids but not polyamines accumulate in macrophages after engulfment, and arginine metabolism does not explain polyamine accumulation

(A) Timeline for Iso-ApoJ co-culture; ApoJ targets were loaded with [^{13}C,^{15}N] amino acids then co-cultured with macrophages.

(B and C) [^{13}C,^{15}N] label was traced in macrophages to identify ApoJ-derived metabolites in amino acids (B) and polyamines (C).

(D) Timeline to trace arginine flux; following co-culture with ApoJ targets, macrophage medium was switched to medium containing [$^{13}C_6$,$^{15}N_4$] arginine.

(E–G) Relative flux was calculated by comparing the fraction of [^{13}C,^{15}N] isotopologue in a downstream metabolite with the fraction in its upstream precursor. Dashed line shows baseline of control no-target macrophages.

(E) Relative ratio to indicate arginase activity.

(F) Relative ratio to indicate ODC1 activity.

(G) Relative ratio to indicate spermidine synthase activity. n = 4/group. LPS-primed peritoneal macrophages were used for all experiments. Data are shown as mean ± SEM; **p < 0.01, ***p < 0.001.

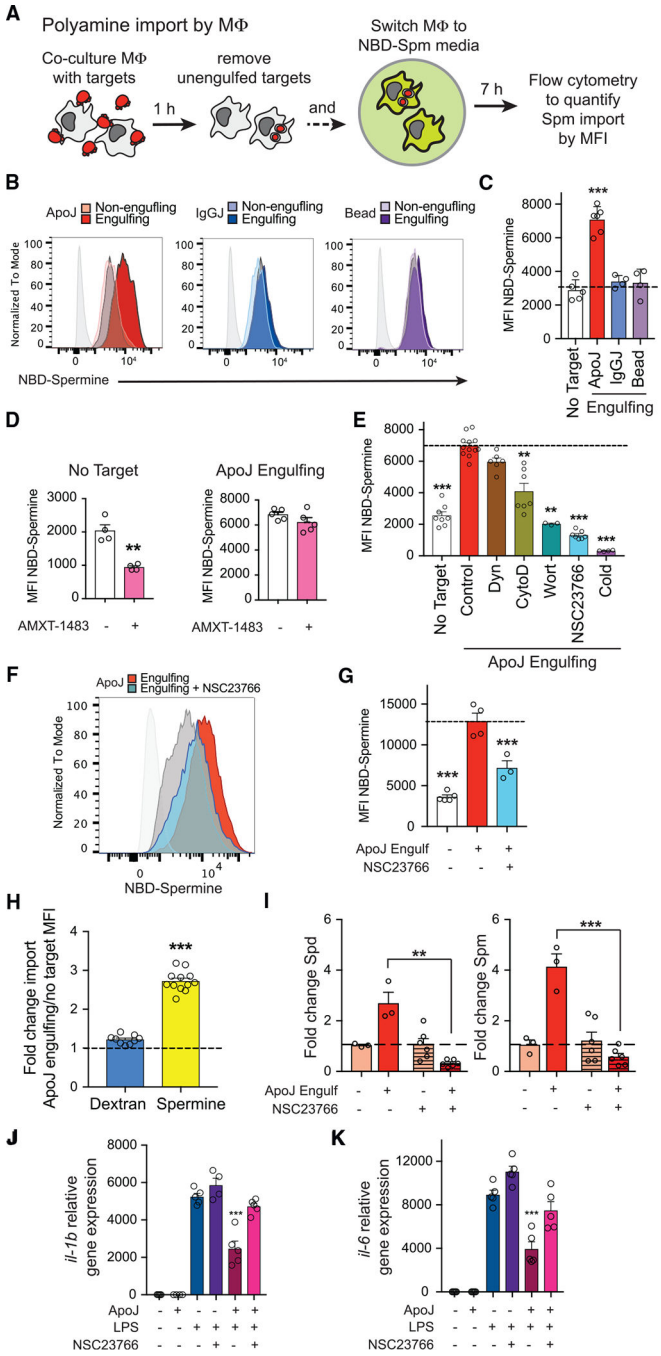

Figure 4. Efferocytosis increases polyamine import via a Rac1 and PI3 kinase-dependent mechanism, leading to polyamine accumulation and IL-1β suppression

(A) Timeline to track polyamine import; following co-culture with targets, macrophage medium was switched to medium containing fluorescent spermine (NBD-spermine).

(B and C) Polyamine import in response to ApoJ (red), IgGJ (blue), and beads (purple).

(B) Representative histogram plots following target co-cultures: engulfing (dark color), non-engulfing (light color), and no-target control (dark grey). Macrophages without NBD-spermine shown in light grey.

(C) Mean fluorescence intensity (MFI) of NBD-spermine quantified for engulfing macrophages after 7 h. n = 4–6.
(D) Effect of AMXT-1483 pre-treatment on NBD-spermine import; MFI of NBD-spermine quantified for control and ApoJ-engulfing macrophages after 7 h. n = 4–5.
(E) Effect of inhibitor pre-treatment on import of NBD-spermine; MFI of NBD-spermine quantified after 7 h. n = 3–12.
(F and G) Spermine import *in vivo*. Naive mice were given IP injections of ApoJ, followed by NSC23766 1 h later at 5 mg/kg, followed by NBD-spermine. (F) Representative histogram of NBD-spermine import by engulfing (dark red), engulfing + NSC23766 (light blue), and no-target control macrophages (dark grey). Macrophages without NBD-spermine are shown in light grey. (G) MFI of NBD-spermine quantified after 5 h.
(H) Import of NBD-spermine compared with import of AF647-dextran after efferocytosis. n = 8–12.
(I) Macrophages were cultured ± ApoJ for 1 h, ± NSC23766 medium for 7 h, then sorted by FACS into non-engulfing and engulfing populations. Macrophage metabolites were assessed using UHPLC-MS shown as fold change relative to the no-target group. n = 3–6.
(J and K) BMDMs were cultured alone or co-cultured with ApoJ. After removal of ApoJ, BMDMs were treated with control media, LPS, or LPS + NSC23766. RNA was collected 6 h later and (J) *il-1b* or (K) *il-6* expression was assessed by RT-PCR, normalized to *b2m* expression. n = 4–5. Data are shown as mean ± SEM; **p < 0.01, ***p < 0.001.

KEY RESOURCES TABLE

REAGENT or RESOURCE	SOURCE	IDENTIFIER
Antibodies		
Anti-mouse CD45	BD	30-F11; RRID:AB_394610
Anti-mouse CD45.1	Invitrogen	A20; RRID:AB_1582228
Anti-mouse CD45.2	BioLegend	104; RRID:AB_313442
Anti-mouse Ly6G	BioLegend	1A8; RRID:AB_1877212
Anti-mouse F4/80	Invitrogen	BM8; RRID:AB_469653
Anti-mouse CD64	BioLegend	X54-5/7.1; RRID:AB_1595539
Anti-mouse CD11b	Invitrogen	M1/70; RRID:AB_953558
Anti-mouse CD16/CD32	Invitrogen	93; RRID:AB_467133
Anti-mouse CD88	BioLegend	20/70; RRID:AB_10896758
Anti-human CD3	BioLegend	UCHT1; RRID:AB_314055
Anti-human CD45	BD	HI30; RRID:AB_395874
Anti-human HLA-DR	BD	G46-6; RRID:AB_2732055
Biological samples		
Blood from healthy human donors	National Jewish Health	IRB approval No. Hs-1285
Chemicals, peptides, and recombinant proteins		
RPMI 1640 Medium	Corning	15040CV
Penicillin/Streptomycin/L-Glutamine	Sigma-Aldrich	G6784
DAPI	BioLegend	422801
HEPES	Corning	25-060-Cl
Sodium Pyruvate	Gibco	11360-070
GemCell U.S. Origin Fetal Bovine Serum	GeminiBio	100-500
5(6)-TAMRA,SE, mixed isomers	Invitrogen	C1171
Flash Red PS/DVB-COOH·(660,690) carboxyl polystyrene beads, 5μm	Bangs Laboratories Inc.	FCFR008
1-Palmitoyl-2-oleoyl-sn-glycero-3-phospho-L-serine (POPS)	Avanti Polar Lipids	840034P
1-palmitoyl-2-oleoyl-glycero-3-phosphocholine (POPC)	Avanti Polar Lipids	850457C
HBSS	Gibco	14175103
30% BSA Solution	Sigma-Aldrich	A8577
EDTA, pH 8.0	Invitrogen	15575020
Lipopolysaccharide, e-coli-O11:B4-derived (LPS)	List Labs	#201
Phosphate Buffered Saline, 1X (PBS)	Gibco	20012027
0.5% Trypsin-EDTA, 10X	Gibco	15400054
X-Vivo 10 Serum-free Hematopoietic Cell Medium	Lonza	04-380Q
Pooled human serum	National Jewish Health	N/A
Cell-free amino acid mixture - 13C, 15N	Sigma-Aldrich	767964
L-ARGININE:HCL (13C6, 99%; 15N4, 99%)	Cambridge Isotope Laboratories	CNLM-539-H-PK
RPMI 1640 Medium for SILAC	Thermo Scientific	88365

REAGENT or RESOURCE	SOURCE	IDENTIFIER
Fetal Bovine Serum - Dialyzed	Sigma-Aldrich	F0392
AMXT-1483	Aminex Therapeutics	N/A
Cytochalasin D	Invitrogen	PHZ1063
NSC23766 trihydrochloride	Sigma-Aldrich	SML0952
Wortmannin	Sigma-Aldrich	W1628
N(1)-Methylspermine nitrobenzoxadiazole conjugate 5 (NBD-Spermine)	Aminex Therapeutics	N/A
Critical commercial assays		
FITC Annexin V Apoptosis Detection Kit I	BD Pharmingen	556457
Deposited data		
Metabolomics data	Metabolomics Workbench NMDR	Project ID: PR001268
Experimental models: Cell lines		
Jurkat, clone E6-1	ATCC	TIB-152
Experimental models: Organisms/strains		
C57BL/6J (WT) mice	Jackson Labs	000664
CCR2KO mice	Jackson Labs	004999
DsRed.T3 mice	Nagy/Jackson Labs	006051
B6 CD45.1 mice	Jackson Labs	002014
Oligonucleotides		
Taqman primers: il1b	Applied Biosystems	4331182/Mm99999061_mH
Taqman primers: il6	Applied Biosystems	4331182/ Mm00446190_m1
Taqman primers: b2m	Applied Biosystems	4331182/ Mm00437762_m1
Software and algorithms		
Image J	NIH	https://imagej.nih.gov/ij/
FlowJo	TreeStar	Version 10
Prism	GraphPad	Version 7
Adobe Illustrator	Adobe	CC 2018
Other		
Genotyping service	Transnetyx	N/A